Continuous Polymerization in Tubular Reactors with Prepolymerization: Analysis Using Two-Dimensional Phenomenological Model and Hybrid Model with Neural Networks

André L. Nogueira,[1] Liliane M. F. Lona,[1] Ricardo A. F. Machado[2]

[1]*Departamento de Processos Químicos, Faculdade de Engenharia Química, Universidade Estadual de Campinas–Unicamp, CEP 13081-970, Campinas, São Paulo, Brazil*
[2]*Departamento de Engenharia Química, Universidade Federal de Santa Catarina, P.B. 476, CEP: 88010-970, Florianópolis, Santa Catarina, Brazil*

Received 17 March 2003; accepted 1 July 2003

ABSTRACT: Continuous polymerization processes have advantages when large amounts of product are required; moreover, higher quality can be obtained because of the elimination of variability between batches. Tubular reactors are economically attractive because of their simple geometry and high heat exchange area; however, they are not commonly used for commercial purposes, mainly because of the large radial profiles. This study elucidates the operation of this kind of reactors in three different ways: first a detailed two-dimensional mathematical model was developed, in which a complete visualization of all axial and radial profiles is possible, allowing a safe analysis at different operating conditions. In a second step a system composed of a continuously stirred tank reactor in series with a tubular reactor was used. A reduction in radial profiles can be clearly observed when prepolymerization is taken into account, improving both the homogeneity and the end properties of the polymer. In a third approach neural networks (NNs) were used in parallel with a one-dimensional model. The objective of this study was to illustrate how NNs can improve the prediction capability when it is not possible to build a reliable model because of uncertainties in parameters and incomplete knowledge of the system. The NNs generated good results, showing that the hybrid model was able to accurately simulate the reactor, even when uncertainty in kinetic and diffusional parameters was imposed to the model. © 2003 Wiley Periodicals, Inc. J Appl Polym Sci 91: 871–882, 2004

Key words: polymerization; tubular reactor; neural networks; modeling; simulations

INTRODUCTION

Continuous polymerization processes offer economic advantages when large amounts of polymer are produced or when slight variations in polymer grade are required. In addition, they are able to provide a higher quality polymer because of the elimination of variability between batches.[1] Tubular reactors are economically attractive because their simple shape lowers fixed and operating costs. The large surface area for heat exchange is particularly advantageous for polymerization reactions because of their high exothermicity. In spite of these advantages, tubular reactors are not commonly used for commercial production of polymers mainly because of the large radial gradients inside the reactor at high conversions. These gradients broaden the residence time distribution of the chains, resulting in a polymer with heterogeneous properties. An alternative to overcome these disadvantages is to carry out monomer prepolymerization before feeding the tubular reactor.[2,3] Therefore, a continuous two-stage polymerization system, composed of a continuously stirred tank reactor (CSTR, where monomer prepolymerization takes place) associated in series with a tubular reactor (to carry out the reaction until high conversions), offers special advantages, such as high production capability and polymer quality enhancement.

The study presented in this article is concerned with the mathematical modeling and numerical simulation of a solution polymerization reaction carried out in a continuous two-stage system composed of a CSTR in series with a tubular reactor. Taking into account the physicochemical characterization of the polymer, phenomenological models were developed for each one of the reactors, and the effects of prepolymerization on the behavior of the tubular reactor and polymer properties were analyzed. The influence of temperature, solvent, and initiator concentration on the behavior of the tubular reactor was also studied.

Correspondence to: L. Lona (liliane@feq.unicamp.br).
Contract grant sponsor: Fundação de Amparo à Pesquisa no Estado de São Paulo (FAPESP).

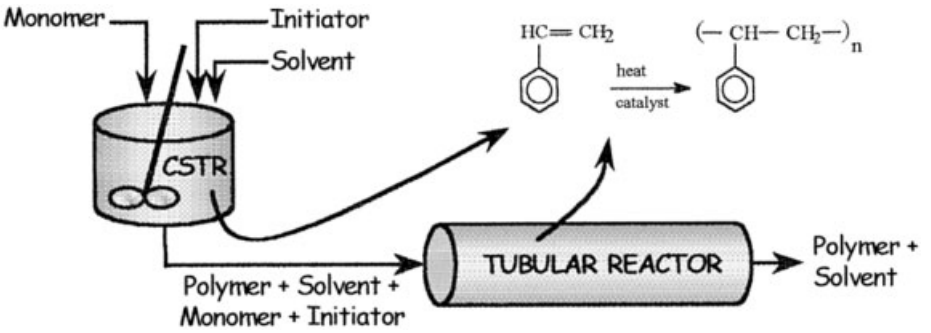

Figure 1 Schematic of a continuous two-stage reaction system.

Modeling of polymerization processes is limited by the lack of sufficient knowledge of the kinetics and transport phenomena of these reaction systems. Moreover, the difficulty in expressing these phenomena through mathematical equations and the large number of diffusional and kinetic parameters that should be estimated have also been a hindrance to the development of accurate polymerization models. An alternative for supplying process knowledge and simplifying the mathematical solution of these models is the application of artificial intelligence techniques such as neural networks (hybrid modeling).

In the area of chemical engineering, neural networks can be used for failure diagnosis in industrial plants, dynamic and steady-state modeling,[4–8] process parameter estimation,[9] identification systems,[10] processes control,[11] sensor data and composition analysis,[12] quality product prediction,[13] optimization,[14–17] and process analysis,[18] among other uses.

Hybrid models can be developed by applying neural networks in series (parameter estimation) or in parallel (process parameter correction) with the phenomenological model. In the latter architecture, the neural network and the phenomenological model output are combined to establish a global output for the hybrid model. In this case, the neural network is trained with the difference between experimental data and phenomenological model results, which compensates for any uncertainties regarding these complex processes.

This article also covers the development of a hybrid model with neural networks (in parallel) to accurately simulate the continuous two-stage polymerization system mentioned before, even when the deterministic model is not sufficiently precise because of uncertainties regarding the parameters of the model. The aim of this hybrid modeling is to illustrate the power of this computational tool in enhancing the predictive capability of pure phenomenological models for polymerization systems.

REACTION SYSTEM AND KINETIC MECHANISM

The continuous reaction system considered in this study is composed of a stirred tank reactor (where prepolymerization takes place) in series with a tubular reactor to carry out the reaction until high conversions, according to Figure 1.

Styrene solution (toluene) polymerization by free radicals, initiated chemically by 2′2-azobisisobutyronitrile (AIBN), was chosen as the case study, specifically because of the great availability of kinetic data in literature. The kinetic mechanism assumes the following reaction steps:

Chemical initiation

$$I \xrightarrow{k_d} 2R^{\bullet}$$

$$R^{\bullet} + M \xrightarrow{k_i} P_1^{\bullet}$$

$$k_d = 1.0533 \times 10^{15} \exp\left(\frac{-15488.33}{T}\right) \qquad (1)$$

(reported by Souroush and Kravaris[19]).

Thermal initiation

$$3M \xrightarrow{\Delta k_{ti}} 2P_1^{\bullet}$$

$$k_{ti} = 1.99 \times 10^{6} \exp\left(\frac{-14842}{T}\right) \qquad (2)$$

(reported by Cutter and Drexler[20]).

Propagation

$$P_n^{\cdot} + M \xrightarrow{k_p} P_{n+1}^{\cdot}$$

$$k_p = 1.051 \times 10^7 \exp\left(\frac{-3577}{T}\right) \tag{3}$$

(reported by Hui and Hamielec[21]).

Chain transfer to monomer

$$P_n^{\cdot} + M \xrightarrow{k_{trm}} D_n + M^{\cdot}$$

$$M^{\cdot} + M \xrightarrow{k'_{trm}} P_1^{\cdot}$$

$$k_{trm} = 2.31 \times 10^6 \exp\left(\frac{-6377}{T}\right) \tag{4}$$

(reported by Husain and Hamielec[22]).

Chain transfer to solvent

$$P_n^{\cdot} + S \xrightarrow{k_{trs}} D_n + S^{\cdot}$$

$$S^{\cdot} + M \xrightarrow{k'_{trs}} P_1^{\cdot}$$

$$k_{trs} = (5.0 \times 10^{-5}) k_p \tag{5}$$

(reported by Kricheldorf[23]).

Termination by combination

$$P_n^{\cdot} + P_m^{\cdot} \xrightarrow{k_{tc}} D_{n+m}$$

$$k_{tc} = 1.255 \times 10^9 \exp\left(\frac{-844}{T}\right) \tag{6}$$

(reported by Hui and Hamielec[21]).

Assuming that reaction rates are independent of chain length (long-chain hypothesis) and that chain life time is short enough (quasi-steady-state assumption), a constant value can be assumed for the increasing polymer chain concentration during the reaction:

$$[P^{\cdot}] = \left(\frac{2fk_dC_i + 2k_{ti}C_m^3}{k_{tc}}\right)^{0.5} \tag{7}$$

Dependency of diffusion on termination and propagation rates (gel and glass effects, respectively) are also included in the kinetic mechanism considered in this model. Typical empirical[21,24] and semiempirical[25] correlations were utilized to express the diffusional limitations, and a comparison between these correlations was made. Variation in initiator efficiency (cage effect) attributed to diffusional limitations was not included in the model because solution polymerization is considered. The AIBN efficiency factor was maintained constant at 0.58 throughout the reaction.[19,26]

MATHEMATICAL MODEL AND NUMERICAL SIMULATION

Deterministic model

According to Lynn and Huff,[2] and Husain and Hamielec,[3] the use of a CSTR to carry out monomer prepolymerization produces less-pronounced radial gradients inside tubular reactors, providing polymers with more homogeneous properties. The present work evaluates and compares the behavior of continuous single (tubular reactor only) and two-stage (CSTR in series with a tubular reactor) polymerization systems through numerical simulation showing three-dimensional graphs for important variables of the system.

The CSTR (prepolymerization) mathematical model uses the steady-state operation, isothermal system, and perfect mixing hypothesis. Because of the steady-state assumption, a set of nonlinear algebraic equations was obtained. The CSTR model was numerically solved using Newton's method.

For the tubular reactor, two mathematical models were elaborated with different purposes in mind, one of which is a simplified model (one-dimensional), developed to study the general profiles obtained for the main process variables when different initiators are used to chemically initiate styrene solution polymerization. The impact of using different correlations to express diffusional limitations is also analyzed with this model.

This phenomenological model assumes plug flow throughout the reactor [constant axial velocity in all radial directions (PFR model)] and estimates only axial variations in the process variables. Steady-state operation, a nonisothermal system, and negligible axial and radial diffusion were also assumed. The plug flow assumption reduces mass, energy, and polymer moments balances (for dead chains) to a set of nonlinear first-order ordinary differential equations, which was numerically solved using the Runge–Kutta–Gill method. The equations obtained from mass and poly-

mer moments balances have the generic form presented below. Live polymer moments equations are exactly the same as those obtained in the realistic (two-dimensional) approach [eqs. (14)–(16)].

$$\frac{d\psi}{dZ} = R_\psi \frac{A\rho}{Q} \tag{8}$$

where ψ is a generic variable that can represent C_m, C_i, C_s, μ_0, μ_1, or μ_2.

The energy balance equation is shown below:

$$\frac{dT}{dZ} = \frac{\left[\Delta H k_p [P^\cdot] C_m \pi \left(\frac{Di}{2}\right)^2 - h\pi Di(T - T_c)\right]}{QCp} \tag{9}$$

The second mathematical model for the tubular reactor assumes a more realistic situation, in which radial and axial gradients are taken into account. The two-dimensional model was developed mainly to analyze the influence of prepolymerization on radial gradients inside the tubular reactor. This realistic model assumes that axial velocity changes with radial direction, producing axial and radial profiles in the tubular reactor. Steady-state operation, a nonisothermal system, heat and mass radial diffusion, and molecular diffusion according to Fick's law were assumed in the realistic modeling. Variation in viscous heat dissipation, radial velocity, radial pressure gradient, and angular parameters were assumed to be negligible. These assumptions resulted in a set of nonlinear second-order partial differential equations composed of mass, energy, and polymer moments (for live and dead chains) balances. The equations obtained from mass balances are shown below.

Monomer consumption

$$\frac{\partial C_m}{\partial Z} = \frac{\left[D\left(\frac{\partial^2 C_m}{\partial r^2} + \frac{1}{r}\frac{\partial C_m}{\partial r}\right) - R_{C_m}\right]}{V_z} \tag{10}$$

$$R_{C_m} = 2fk_dC_i + k_p[P^\cdot]C_m + 3k_{ti}C_m^3 + 2k_{trm}[P^\cdot]C_m + k_{trs}[P^\cdot]C_s \tag{11}$$

Initiator consumption

$$\frac{\partial C_i}{\partial Z} = \frac{\left[D\left(\frac{\partial^2 C_i}{\partial r^2} + \frac{1}{r}\frac{\partial C_i}{\partial r}\right) - k_dC_i\right]}{V_z} \tag{12}$$

Solvent consumption

$$\frac{\partial C_s}{\partial Z} = \frac{\left[D\left(\frac{\partial^2 C_s}{\partial r^2} + \frac{1}{r}\frac{\partial C_s}{\partial r}\right) - k_{trs}C_s[P^\cdot]\right]}{V_z} \tag{13}$$

The equations obtained from polymer moments balances (for live and dead chains) are presented below:

Zeroth moment for live polymer chains

$$\lambda_0 = \left(\frac{2fk_dC_i + 2k_{ti}C_m^3}{k_{tc}}\right)^{1/2} \tag{14}$$

First moment for live polymer chains

$$\lambda_1 = \frac{2fk_dC_i + 2k_{ti}C_m^3 + \lambda_0(k_pC_m + k_{trm}C_m + k_{trs}C_s)}{k_{trm}C_m + k_{trs}C_s + k_{tc}\lambda_0} \tag{15}$$

Second moment for live polymer chains

$$\lambda_2 = \frac{2fk_dC_i + 2k_{ti}C_m^3 + k_pC_m(2\lambda_1 + \lambda_0) + \lambda_0(k_{trm}C_m + k_{trs}C_s}{k_{trm}C_m + k_{trs}C_s + k_{tc}\lambda_0} \tag{16}$$

Zeroth moment for dead polymer chains

$$\frac{\partial \mu_0}{\partial Z} = \frac{\left[D\left(\frac{\partial^2 \mu_0}{\partial r^2} + \frac{1}{r}\frac{\partial \mu_0}{\partial r}\right) + k_{trm}C_m\lambda_0 + k_{trs}C_s\lambda_0 + \frac{1}{2}k_{tc}\lambda_0^2\right]}{V_z} \tag{17}$$

First moment for dead polymer chains

$$\frac{\partial \mu_1}{\partial Z} = \frac{\left[D\left(\frac{\partial^2 \mu_1}{\partial r^2} + \frac{1}{r}\frac{\partial \mu_1}{\partial r}\right) + k_{trm}C_m\lambda_1 + k_{trs}C_s\lambda_1 + k_{tc}\lambda_0\lambda_1\right]}{V_z} \tag{18}$$

Second moment for dead polymer chains

$$\frac{\partial \mu_2}{\partial Z} = \frac{\left[D\left(\frac{\partial^2 \mu_2}{\partial r^2} + \frac{1}{r}\frac{\partial \mu_2}{\partial r}\right) + k_{trm}C_m\lambda_2 + k_{trs}C_s\lambda_2 + k_{tc}(\lambda_0\lambda_2 + \lambda_1^2)\right]}{V_z} \tag{19}$$

Because of reactor symmetry, the same boundary conditions associated with mass and polymer moments balances were applied at the center of the reactor and at the reactor wall:

$$\frac{\partial \psi}{\partial r} = 0 \quad (r = 0 \quad \text{and} \quad r = R) \tag{20}$$

From the energy balance, the following partial differential equation was obtained to take into account the heat transfer throughout the tubular reactor:

$$\frac{\partial T}{\partial Z} = \frac{\left[\dfrac{k}{\rho Cp}\left(\dfrac{\partial^2 T}{\partial r^2} + \dfrac{1}{r}\dfrac{\partial T}{\partial r}\right) - \dfrac{\Delta H}{\rho Cp} k_p C_m [P^\cdot]\right]}{V_z} \tag{21}$$

Symmetry in the heat radial profiles was considered:

$$r = 0 \rightarrow \frac{\partial T}{\partial r} = 0 \tag{22}$$

At the reactor wall, the conductive heat transfer was assumed to be equal to the convective heat transfer. The cooling fluid temperature was maintained at a constant value throughout the reactor (equal to the initial polymerization temperature).

$$r = R \rightarrow \frac{\partial T}{\partial r} = -\frac{h}{k}(T - T_c) \tag{23}$$

Applying the hypothesis mentioned previously to the continuity (mass conservation) and Navier–Stokes equations, the following equation for momentum balance was generated:

$$\frac{\partial P}{\partial Z} = \frac{1}{r}\frac{\partial}{\partial r}\left(\mu r \frac{\partial V_z}{\partial r}\right) \tag{24}$$

By twice integrating analytically eq. (24) from reactor wall ($r = R$) to any position inside the tubular reactor toward the center of the reactor ($r = r$), the following expression for the axial velocity was obtained:

$$V_z = \left(\frac{\partial P}{\partial Z}\right)\frac{1}{2}\int_R^r \frac{r}{\mu}\, dr \tag{25}$$

To guarantee a constant mass flux across the tubular reactor, the following equation was introduced into the momentum balance:

$$Q = \int_0^{2\pi}\int_0^R \rho V_z r\, dr\, d\theta \tag{26}$$

Substitution of eq. (26) into eq. (25) provides an equation for pressure drop throughout the tubular reactor:

$$\left(\frac{\partial P}{\partial Z}\right) = -\frac{Q}{\pi \displaystyle\int_0^R \rho r \int_R^r \frac{r}{\mu}\, dr\, dr} \tag{27}$$

Finally, by substituting the pressure drop equation [eq. (27)] into eq. (25), an expression to estimate the axial velocity applicable to any position in the radial direction throughout the tubular reactor was obtained:

$$V_z = -\frac{\dfrac{Q}{2}\displaystyle\int_R^r \frac{r}{\mu}\, dr}{\pi \displaystyle\int_0^R \rho r \int_R^r \frac{r}{\mu}\, dr\, dr} \tag{28}$$

The symmetry at the center of the reactor and no axial flow at the reactor wall led to the following boundary conditions:

$$r = 0 \rightarrow \frac{\partial V_z}{\partial r} = 0 \tag{29}$$

$$r = R \rightarrow V_z = 0 \tag{30}$$

The integral terms in eqs. (27) and (28) were solved numerically using Simpson's rule.

The numerical solution of the realistic (two-dimensional) model was obtained in two steps. The first one constitutes radial term discretization, which reduces the system of partial differential equations into a set of ordinary differential equations n times greater than the original system, where n is the number of discretization points in the radial direction. The orthogonal collocation method was applied for this purpose, changing dimensionless radial derivatives into linear algebraic equations, according to the following equations:

$$\frac{\partial \psi}{\partial \sigma} = \sum_{i=1}^{n+1} A_{ij}\psi_i \tag{31}$$

$$\frac{\partial^2 \psi}{\partial \sigma^2} = \sum_{i=1}^{n+1} B_{ij}\psi_i \tag{32}$$

This discretization technique was also applied under the boundary conditions at the reactor wall ($n + 1$ position) to make feasible numerical solution of the resulting system of ordinary differential equations.

After radial derivative discretization, the nonlinear system of ordinary differential equations obtained was numerically integrated through an implicit integration method (the Adams–Moulton method). The most important characteristic of this implicit integration method is its capability to overcome stiffness problems, frequently reported in modeling and simulation studies on polymerization systems.[27–29]

Because of the strong dependency of the properties of polymeric materials on their molecular weight distributions (MWD), mathematical modeling of these statistical curves becomes an important tool when polymerization systems are simulated. MWD curves are histograms that describe overall properties of polymer chains as a function of a given variable. Histograms that represent the distribution of macromolecules (number and weight) as a function of the number of monomer units in their chains are the most important histograms related to polymer properties.

Different methods to estimate MWD curves are available in the literature. In the present study the method of moments was applied to build the polymer physicochemical characterization model, so that number- and weight-average molecular weights of the polymer and polydispersity index can be predicted.

Usually, the first three moments (zeroth-, first-, and second-order) are enough to describe a polymer. High-order moments are difficult to obtain and are not always useful for describing a given polymer property.[30] The kth moment of live polymer chains is described according to the following equation:

$$\lambda_k = \sum_{n=1}^{\infty} n^k [P_n^{\cdot}] \tag{33}$$

The kth moment of dead polymer chains is described by the following equation:

$$\mu_k = \sum_{n=1}^{\infty} n^k [D_n] \tag{34}$$

Through the relationship among the zeroth-, first-, and second-order moments of live and dead polymer chains, the number-average ($\overline{M}_n$) and weight-average molecular weight ($\overline{M}_w$) can be written as follows:

$$\overline{M}_n = \frac{\mu_1 + \lambda_1}{\mu_0 + \lambda_0} PM \tag{35}$$

$$\overline{M}_w = \frac{\mu_2 + \lambda_2}{\mu_1 + \lambda_1} PM \tag{36}$$

Because live polymer moments are extremely small, they are normally omitted from polymer average molecular weight calculations [eqs. (35) and (36)]. Thus the term μ_1/μ_0 represents the average number of monomer units in the polymer chains and the term μ_2/μ_1 represents the weight-average number of monomer units in the polymer chains.

The polydispersity index (PI), which is an average value referring to the MWD curve breadth, is calculated from the ratio between the weight- and number-average molecular weights of the polymer:

$$PI = \frac{\overline{M}_w}{\overline{M}_n} = \frac{\mu_2 \mu_0}{\mu_1^2} \tag{37}$$

Hybrid model

The hybrid model proposed in this article uses an artificial neural network in parallel with the phenomenological model of the tubular reactor. Neural network outputs are added to the simulation results obtained for the tubular reactor to enhance the prediction capability of its phenomenological model. The exit conditions for the CSTR model are used to provide the input data for the hybrid model.

In this model structure, the neural network is responsible for estimating deviations between the phenomenological model predictions and reliable data (e.g., experimental data or data obtained from a pilot or industrial plant).

For the phenomenological model, the one-dimensional model was used. The plug flow assumption mimics the lack of detailed knowledge of process rheology and, consequently, the transport phenomena related to it. To mimic a case for which not enough knowledge of the polymerization process is available, the kinetics were also simplified in this one-dimensional model. Chain transfer to solvent and monomer were not considered, no correlations for gel and glass effect were used, and an initiator efficiency of 100% ($f = 1.0$) was assumed. The main purpose of this simplification is to mimic a real situation in which not enough information about the polymerization system is available.

The training data used in the learning step constitute deviations between the results obtained with this simplified tubular reactor model and experimental data. Therefore for a given operating condition, the trained neural network provides deviations that should be added to the simplified model results (Fig. 2) to enhance its prediction capabilities.

The artificial neural network applied to the hybrid model is a feedforward network that uses the backpropagation training algorithm (gradient-descent techniques). Network topology includes complete neuron interconnectivity, an input layer composed of seven neurons, two hidden layers, and an output layer of four neurons. A sigmoidal function was used for

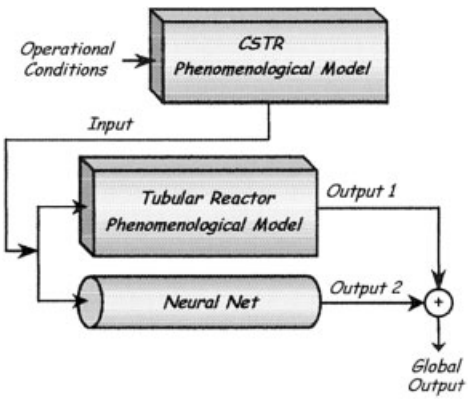

Figure 2 Structure of the hybrid model.

signal processing through the layers. Input and output values of the neural network were normalized between 0.2 and 0.8 to avoid the saturation region of the activation function used.

Input neurons represent monomer, solvent and initiator consumption, temperature, mass flow, polymer weight-average molecular weight, and polydispersity index. The output neurons represent measurements for the mean square deviations between the results obtained from the simplified model and experimental data for monomer and initiator consumption (X_M and X_I, respectively), polymer M_w, and PI. The following generic eq. (38), in which ψ is the generic process variable described earlier, was used to calculate the mean square deviations:

$$\delta_\psi = \left(\frac{\psi_{\text{exp}} - \psi_{\text{simplified}}}{\psi_{\text{exp}}} \right)^2 \tag{38}$$

The second-order exponent in the above equation guarantees a positive result, whereas division by the experimental term renders the deviation magnitude uniform.

It was observed that 25 neurons for each hidden layer was a reasonable number to provide good predictions.

Because of the lack of enough experimental data for coherent network training, the realistic two-dimensional model was used to represent the experimental/industrial data. Thus, for the case studied, the hybrid model should be able to accurately simulate the tubular reactor and generate results compatible with those obtained from the realistic two-dimensional phenomenological model developed for this equipment.

RESULTS AND DISCUSSION

Prepolymerization effect

The study of the prepolymerization effect was performed to compare radial gradients of process variables when continuous single and two-stage polymerization systems were used to carry out the same reaction.

In the first study two reaction systems of equal volume were used to simulate styrene polymerization in toluene. One of them was a single tubular reactor (without prepolymerization) with a reaction volume of V_t (with $Di = 0.0254$ m). The second reaction system was composed of a CSTR with a reaction volume of $0.2 \times V_t$, associated in series with a tubular reactor with a reaction volume of $0.8 \times V_t$. The operating conditions used were a solvent volumetric fraction of 0.2, an initial initiator concentration of 0.005 mol/L, an initial polymerization temperature of 350 K, a constant cooling temperature of 350 K, and a mass flow of 0.0003 kg/s.

Figure 3(a) shows that the CSTR (for prepolymerization) significantly reduced the radial gradients of axial velocity throughout the tubular reactor. Because of the higher viscosity of the reaction mixture fed into the tubular reactor when prepolymerization was used, lower velocities were observed inside the reactor, leading to a narrower residence time distribution for macromolecules.

The profiles of temperature inside the tubular reactor for each reaction system showed considerably different behavior [Fig. 3(b)]. In the system with prepolymerization the generation of a large amount of heat at the beginning of the reaction (characteristic of chain-addition polymerization reactions) occurred within the CSTR, resulting in lower temperatures and smooth radial profiles throughout the tubular reactor. A higher temperature was clearly visible at the reactor inlet for the single polymerization system.

Monomer and initiator consumption were strongly influenced by axial velocity and reactor temperature, so less-pronounced profiles for monomer and initiator consumption were observed when prepolymerization was assumed (not shown).

Figure 3(c) shows that the evolution of polymer weight-average molecular weight in the tubular reactor varied considerably between the reaction systems studied. In the single polymerization system faster polymer chain growth, characteristic of this kind of reaction, was observed at the tubular reactor entrance. In the two-stage polymerization system this occurred within the CSTR.

Figure 3(d) shows that in the two-stage polymerization system, less-pronounced radial gradients and a lower polydispersity index were obtained throughout the tubular reactor.

Although monomer prepolymerization reduced radial gradients throughout the tubular reactor, different values were obtained at the reactor exit for all variables analyzed. This means that different operating conditions should be used in the two-stage polymerization system to achieve conversion and polymer

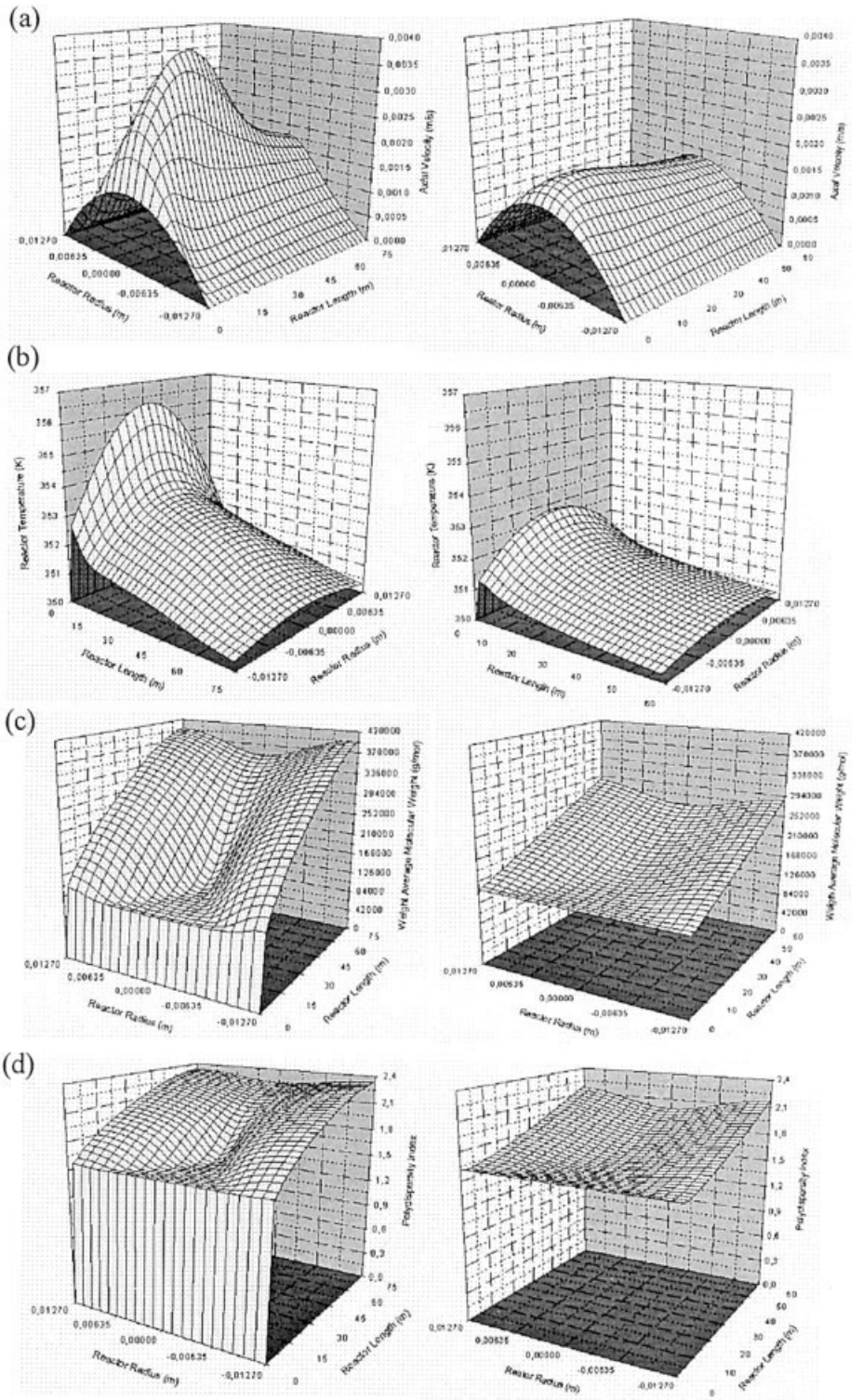

Figure 3 Profiles of (a) axial velocity, (b) reactor temperature, (c) polymer weight-average molecular weight, and (d) polydispersity index in the tubular reactor for single (left) and two-stage (right) polymerization reaction systems.

properties similar to those obtained in the single-reaction system.

Parametric analysis

Different solvent fractions, polymerization temperatures, and initiator concentrations were tested using the two-dimensional model developed for the tubular reactor ($L = 75$ m).

Solvent volumetric fractions of 20, 30, 40, and 60% were studied through simulations. Results show that when the solvent fraction was increased, less-pronounced radial gradients were observed for all pro-

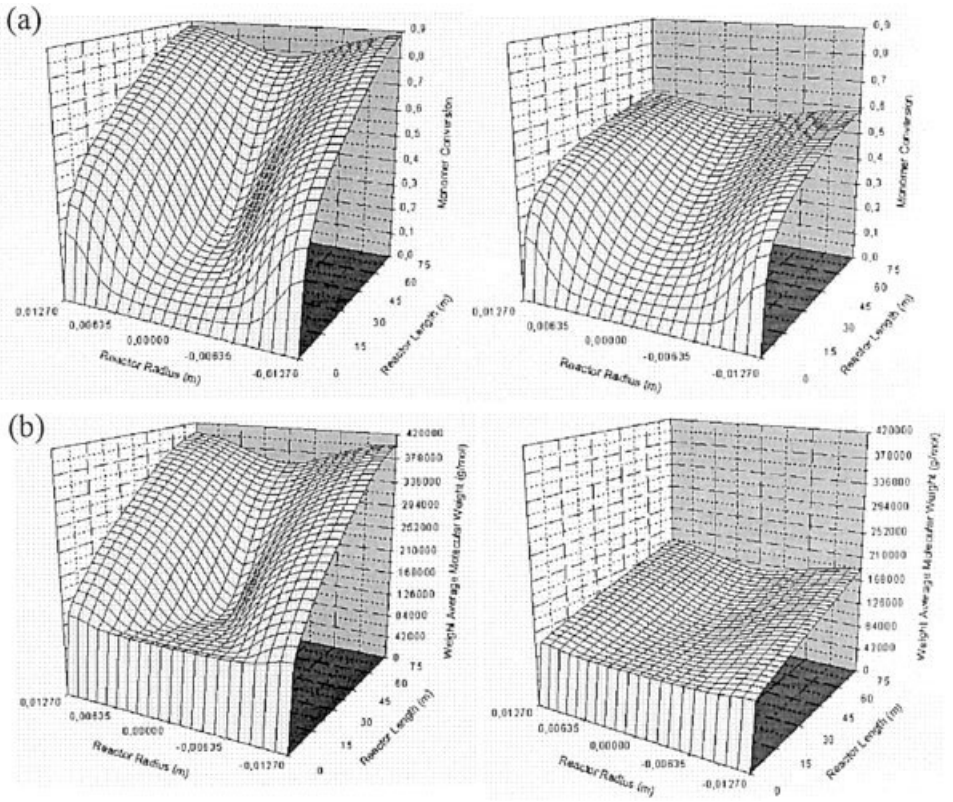

Figure 4 Profiles of (a) monomer conversion and (b) polymer weight-average molecular weight in the tubular reactor for volumetric solvent fractions of 20% (left) and 40% (right).

cess variables (Fig. 4), as expected, attributed to the decrease in viscosity as the solvent fraction increased, which resulted in less-elongated axial velocity profiles. According to Figure 4(a), as the solvent fraction was increased from 20 to 40%, the monomer consumption rate underwent a considerable reduction.

The decrease in monomer consumption rate resulted in a lower release of heat by propagation reaction and, consequently, lower temperatures were observed inside the reactor. This reduction in the propagation reaction rate can be verified by the dramatic decrease in the number- and weight-average molecular weights [Fig. 4(b)]. It is explained by the reduction in the diffusional limitations when higher solvent fractions were used (the free volume increased), which facilitated termination of the chains and maintained a more constant value for radical concentration. In addition, the chain transfer to solvent was also increased. The polydispersity index was also reduced when more solvent was used.

To study the effect of polymerization temperature, the cooling fluid temperature was assumed to be equal to the initial polymerization temperature. Styrene solution polymerization with a solvent volumetric fraction of 30% and initial temperatures (at the reactor entrance) of 345, 350, and 355 K were simulated.

Results show that the higher the polymerization temperature, the faster the consumption of reactant, which is in accordance with kinetic theory. The increase in monomer consumption by propagation reaction resulted in higher generation of heat attributed to the exothermicity of the reaction. Because of the assumption of equality between the cooling and the initial polymerization temperatures, heat release from the reaction system was more difficult when a higher initial temperature was assumed. As a consequence, a higher temperature was obtained inside the tubular reactor, resulting in a total initiator consumption. This occurred as a result of the low initial value chosen for this variable in the simulations (C_{i0} = 0.005 mol/L). Total initiator consumption resulted in a constant increase in the weight-average molecular weight and polydispersity index, equivalent to those observed on the left side of Figure 3(c) and (d), respectively.

The model is also in accordance with the fact that temperature and initiator concentration have similar effects on reactor behavior. The increase in initiator concentration from 0.005 to 0.015 mol/L resulted in a drastic reduction in the polymer average molecular weight. A lower polydispersity index was also obtained.

Different empirical[19,20] and semiempirical[21] correlations to express the gel effect in solution polymerization of styrene in tubular reactors were tested. Results show that when an empirical correlation was used in a nonisothermal system, strong discontinuities were observed in the temperature profile when the gel effect was assumed (i.e., within the conversion range of

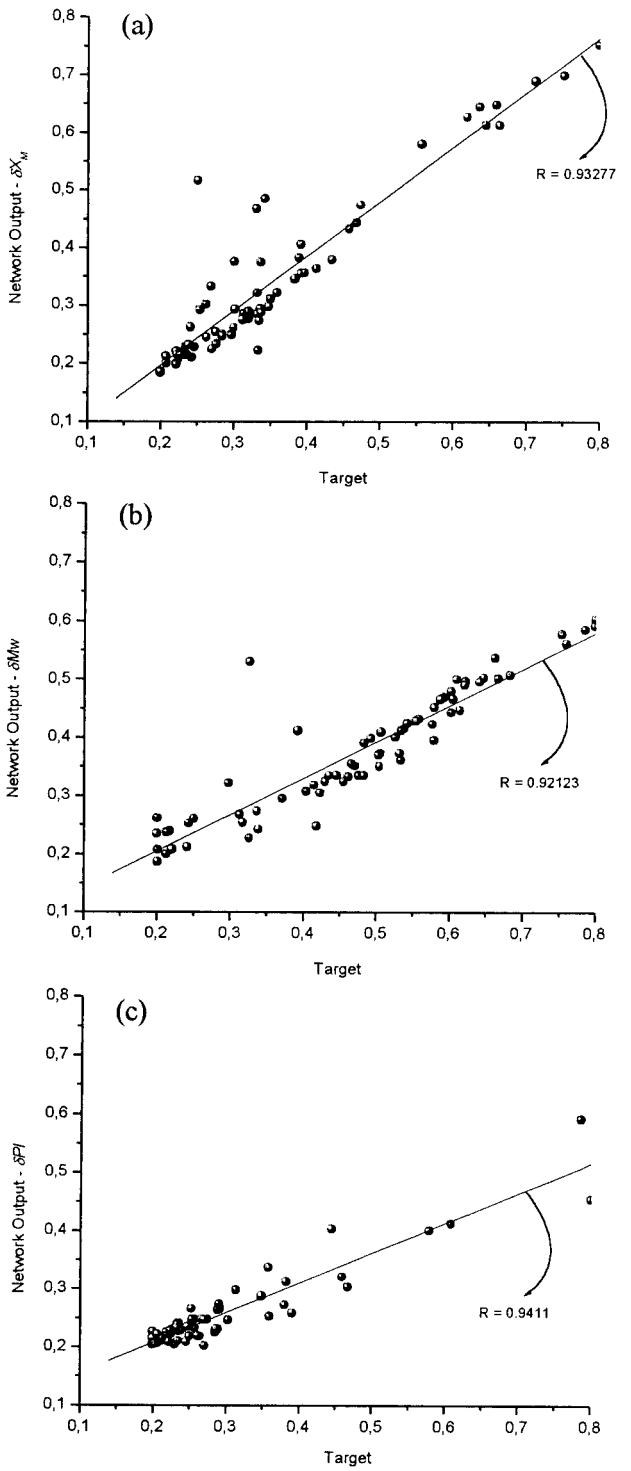

Figure 5 Neural network performance for test patterns of (a) δX_M, (b) δM_w, and (c) δPI.

the validity of gel effect), so semiempirical correlations are more appropriate. Equivalent final conversion values (at the reactor outlet) were obtained for all correlations used in simulations, although the profiles in the reactor were considerably different. The polymer average molecular weight and polydispersity index had different final values and profiles throughout the reactor.

Finally, benzoyl peroxide and AIBN were tested as chemical initiators for solution polymerization of styrene in tubular reactors. Results indicated that, for a given temperature, initiators with a lower half-life time (i.e., AIBN) generated more heat near the reactor entrance. Lower polymer average molecular weight and a higher polydispersity index were obtained when AIBN was used in the simulations.

Neural network performance

Training and test sets of patterns were generated through simulations with random operating conditions in the training range for each process variable involved. For network training, 80,000 epochs were necessary to obtain a mean square error of 0.000076. A learning rate of 0.3 was used in this step.

The quality of the network response was verified through observations of the angular coefficient evaluated from the plot of neural network predictions versus output targets (Fig. 5). The angular coefficient (correlation coefficient) obtained from training and test plots, shown in Table I, indicates the good performance of the neural network for learning and test patterns.

Using test patterns, the predictions obtained with hybrid and phenomenological models (simplified and realistic) for monomer conversion [Fig. 6(a)], polymer weight-average molecular weight [Fig. 6(b)], and polydispersity index [Fig. 6(c)] show good agreement between hybrid and two-dimensional model results. This suggests that the hybrid model applied in parallel with a neural network is a promising alternative to improve the prediction capability of conventional mathematical models of polymerization systems. In other words, despite the simplifications made in the one-dimensional model for the tubular reactor, the neural network was able to overcome the lack of kinetic and phenomenological knowledge, increasing the prediction capability of the model.

CONCLUSIONS

This research addressed the behavior of a continuous polymerization system composed of a continuously stirred tank reactor (prepolymerization) in series with

TABLE I
Neural Network Performance for Training and Test Patterns

	Correlation coefficient	
Output neuron (deviations)	Training	Test
δX_M	0.99774	0.93277
δX_I	0.99771	0.97631
δM_W	0.99320	0.92123
δPI	0.98319	0.94110

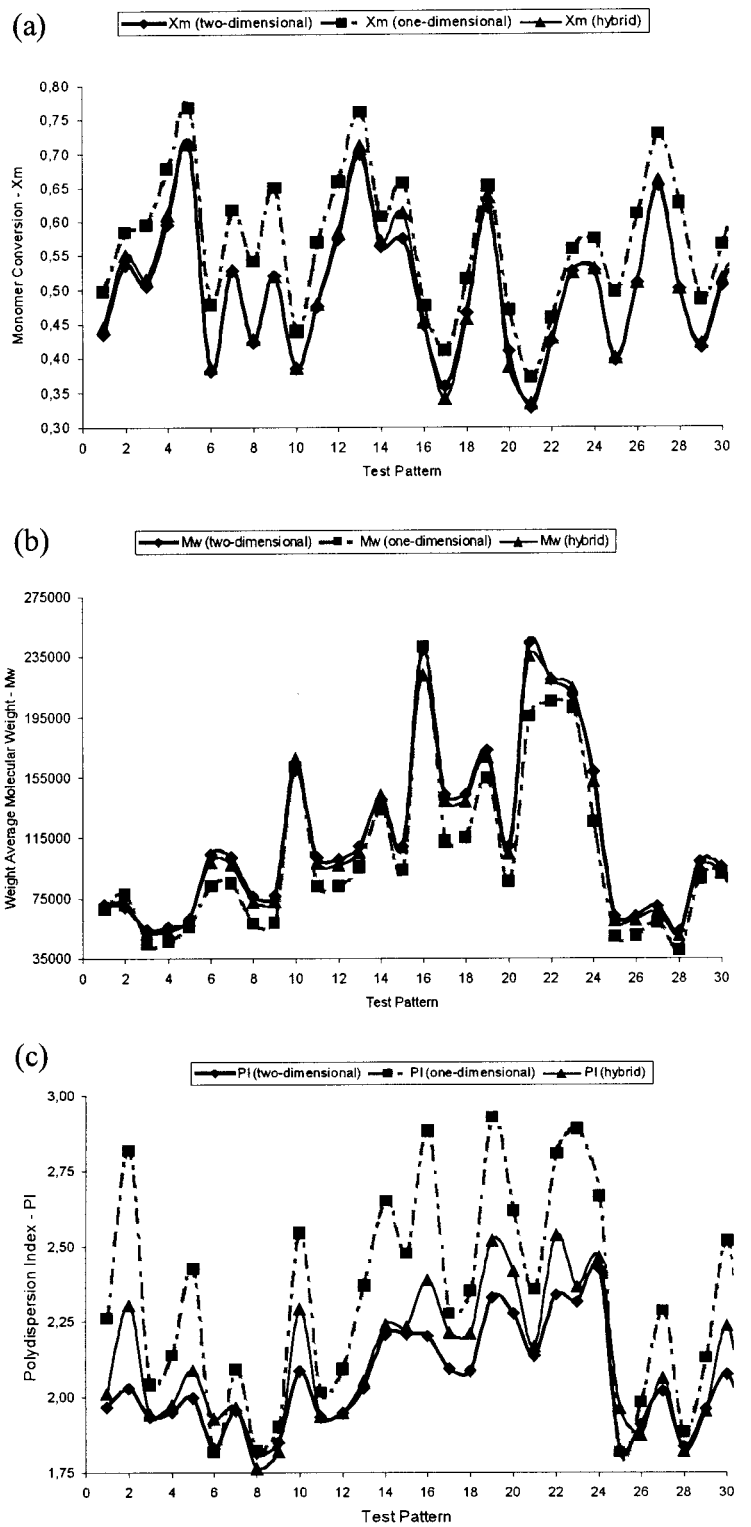

Figure 6 Comparison of (a) the monomer conversion, (b) polymer weight-average molecular weight, and (c) polydispersity index results obtained for random operating conditions with the simplified, realistic, and hybrid models.

a tubular reactor using a two-dimensional model. With this model, a complete visualization of all axial and radial profiles inside the tubular reactor was possible, allowing a safe analysis of the advantages of using a prepolymerization reactor to improve both the homogeneity and the end properties of the polymer.

This work also proposed a hybrid model with a neural network in parallel as an alternative to improve

the prediction capability when it is not possible to build a reliable phenomenological model attributed to uncertainties in parameters and incomplete knowledge of the system. The results showed that the hybrid model could generate good results, even when there was a serious lack of information about the system.

NOMENCLATURE

A tubular reactor cross-sectional area (m^2)
A_{ij} matrix coefficients for first-order derivative discretization
B_{ij} matrix coefficients for second-order derivative discretization
C_i initiator concentration (mol/L)
C_m monomer concentration (mol/L)
Cp heat capacity (J kg^{-1} K^{-1})
C_s solvent concentration (mol/L)
D molecular diffusion coefficient (m^2/s)
Di tubular reactor diameter (m)
D_x dead polymer chain with x monomer units
f initiator efficiency
h convective heat transfer coefficient (J m^{-2} s^{-1} K^{-1})
I initiator molecule
k conduction heat transfer coefficient (J m^{-1} s^{-1} K^{-1})
k_d initiator decomposition rate constant (s^{-1})
k_i chemical initiation rate constant (L mol^{-1} s^{-1})
k_{ti} thermal initiation rate constant (L^2 mol^{-2} s^{-1})
k_p propagation rate constant (L mol^{-1} s^{-1})
k_{trm} chain transfer to monomer rate constant (L mol^{-1} s^{-1})
k_{trs} chain transfer to solvent rate constant (L mol^{-1} s^{-1})
k_{tc} termination by combination rate constant (L mol^{-1} s^{-1})
L tubular reactor length (m)
M monomer molecule
$M^{\bullet}$ active monomer molecule
M_n number-average molecular weight (g/mol)
M_w weight-average molecular weight (g/mol)
Q mass flow (kg/s)
R_{Cm} reaction rate of monomer consumption (mol L^{-1} s^{-1})
R_ψ generic reaction rate
P reactor pressure (N/m^2)
PI polydispersity index
$P^{\bullet}_x$ live polymer chain with x monomer units
PM monomer molecular weight (g/mol)
r radial coordinate (m)
$R^{\bullet}$ free radical
S solvent molecule
$S^{\bullet}$ active solvent molecule
T reactor temperature (K)
T_c cooling fluid temperature (K)
V_z axial velocity (m/s)
Z axial coordinate (m)

Greek characters

δ_ψ mean square deviation
ΔH heat of polymerization (J/mol)
λ_k kth moment of live polymer chain
μ viscosity of reaction mixture (cP)
μ_k kth moment of dead polymer chain
θ angular coordinate (rad)
ρ density of reaction mixture (g/L)
σ dimensionless radial coordinate
ψ generic variable that can represent C_m, C_i, C_s, μ_0, μ_1, or μ_2

The authors gratefully acknowledge the financial support received from FAPESP (Fundação de Amparo à Pesquisa no Estado de São Paulo).

References

1. Paquet, D. A., Jr.; Ray, W. H. AIChE J 1994, 40, 73.
2. Lynn, S.; Huff, J. E. AIChE J 1971, 17, 475.
3. Husain, A.; Hamielec, A. E. AIChE Symp Ser 1976, 72, 112.
4. Bhat, N.; McAvoy, T. J. Comput Chem Eng 1990, 14, 573.
5. Psichogios, D. C.; Ungar, L. H. AIChE J 1992, 38, 1499.
6. You, Y.; Nikolaou, M. AIChE J 1993, 39, 1654.
7. Bogdan, S.; Gosak, D.; Vasic-Racki, D. Comput Chem Eng 1995, 19, 791.
8. Azevedo, R.; Lima, H. L.; Pinto, J. C. In: Dinâmica e Controle de Reatores Tubulares de Polimerização, Anais do 2° Congresso Brasileiro de Polímeros, São Paulo, Brazil, Oct. 5–8, 1993; pp. 834–839.
9. Karin, M. K.; Rivera, S. L. ESCAPE 1991, 1, s369.
10. Pollard, J. F.; Broussard, M. R.; Garrison, D. B.; San, K. Y. Comput Chem Eng 1992, 16, 253.
11. Tsen, A. Y.; Jang, S. S.; Wong, D. S. H. AIChE Journal 1996, 42, 455.
12. Araújo, P. H. H. H.; Sayer, C.; Cal, J. C.; Asua, J. M.; Lima, E. L.; Pinto, J. C. Lat Am Appl Res 2001, 31, 525.
13. Zhang, J.; Morris, A. J.; Martin, E. B.; Kiparissides, C. Chem Eng J 1998, 69, 135.
14. Kiparissides, C.; Verros, G.; Pertsinidis, A. Chem Eng Sci 1994, 49, 5011.
15. Shang, Y.; Wah, B. W. IEEE 1996, March, 45.
16. Krothapally, M.; Palanki, S. Comput Chem Eng 1997, 21, 463.
17. Nascimento, C. A. O.; Giudici, R. Comput Chem Eng 1998, 22, s595.
18. Savkovic-Stevanovic, J. Comput Chem Eng 1994, 18, 5011.
19. Soroush, M.; Kravaris, C. AIChE J 1993, 39, 1920.
20. Cutter, L. A.; Drexler, T. D. Comput Appl Polym Sci 1982, 13.
21. Hui, A.; Hamielec, A. E. J Appl Polym Sci 1972, 16, 749.
22. Husain, A.; Hamielec, A. E. J Appl Polym Sci 1978, 22, 1207.
23. Kricheldorf, H. R. Handbook of Polymer Synthesis: Part A; Marcel Dekker: New York, 1992.
24. Sacks, M. E.; Lee, S.-I. I.; Biesenberger, J. A. Chem Eng Sci 1973, 28, 241.
25. Marten, F. L.; Hamielec, A. E. ACS Symp Ser 1978, 104, 46.
26. Blavier, L.; Villermaux, J. Chem Eng Sci 1984, 19, 101.
27. Tossun, G. AIChE J 1992, 38, 425.
28. Soliman, M. A.; Aljarboa, T.; Alahmad, M. Polym Eng Sci 1994, 34, 1464.
29. Powell, F. E.; Brooks, B. W. Chem Eng Sci 1995, 50, 837.
30. Ray, W. H. J Macromol Sci Rev Macromol Chem 1972, C8, 1.